Journal of The Electrochemical Society, **151** (8) J62-J68 (2004)
0013-4651/2004/151(8)/J62/7/$7.00 © The Electrochemical Society, Inc.

Interpretation of Electrical Conductance Transition of Hematite in the Spin-Flip Magnetic Transition Temperature Range

G. Patermarakis,[a,z] J. Papaioannou,[b] H. Karayianni,[a] and K. Masavetas[a]

[a]*Laboratory of Physical Chemistry, Department of Materials Science and Engineering, School of Chemical Engineering, National Technical University of Athens, Zografou 157 80, Athens, Greece*
[b]*Laboratory of Physical Chemistry, Department of Chemistry, University of Athens, Panepistimioupolis 157 71, Athens, Greece*

Using polycrystalline pure hematite at frequencies of 100 Hz-100 kHz and temperatures of 190-350 K impedance spectroscopy was employed to investigate the electrical conductance transition and correlate it with magnetic transition occurring within this temperature range. A background of slight impurity donor or acceptor semiconductivity was observed above which a peak of conductivity appeared in the temperature range of magnetic transition. The results suggested that the transition from antiferromagnetically to weak ferromagnetically coupled Fe^{3+} and vice versa takes place through their transformation to uncoupled Fe^{3+} and an equilibrium between these types of coupled and uncoupled pairs of Fe^{3+} is established. A model, thermodynamically sustained, involving bulk concentration of both types of coupled and of uncoupled Fe^{3+} was formulated precisely predicting the dependence of magnetic transition on temperature and the appearance of peaks in both the uncoupled Fe^{3+} concentration and conductivity within the transition temperature range. The conductivity, mainly due to intrinsic semiconductance coming from the activation of uncoupled Fe^{3+}, depends on both temperature and concentration of uncoupled Fe^{3+}. The heretofore elusive semiconductive character of hematite is explained.
 [DOI: 10.1149/1.1768549]

Manuscript received August 11, 2003. Available electronically July 20, 2004.

The crystal structure of hematite, α-Fe_2O_3, is that of corundum, α-Al_2O_3, with a rhombohedral unit cell. Hematite exhibits unusual magnetic properties, which have been extensively studied. Hematite is an antiferromagnetic material at low temperatures. At temperatures higher than the Néel one, $T_N = 956$ K, hematite becomes paramagnetic. Below T_N the material presents a spin-flip transition at temperature T_M (considered $\approx$265 K for coarse crystalline bulk or monocrystalline hematite) called the Morin transition.[1-22] Below T_M the spins of Fe^{3+} belonging to two alternative sublattices are oriented parallel to the trigonal [111] axis (*c* axis) and the material behaves as a uniaxial antiferromagnetic (AF) one. Above T_M the spins lie in the basal (111) plane, perpendicular to the [111] axis except for a slight spin canting, $\approx$1 min of the arc, out of the basal plane which causes a small net weak ferromagnetic (WF) moment. This transition arises from two competitive anisotropy components of total energy with comparable magnitudes, opposite signs, and different temperature dependences:[1-3] (*i*) the local fine structure anisotropy component which is positive arises from the higher order of spin-orbit coupling of the individual cations and is quite short, the range falls off exponentially with spin separation distance and (*ii*) the long-range magnetic dipolar anisotropy component which is negative and falls off only as the inverse cube of the dipole separation distance. At T_M a change of total energy sign occurs which is responsible for the spin-flip transition.

The transition is affected, or even suppressed, by different structures and natural parameters, like grain size,[4,5] thus T_M is reduced with decreasing particle size and tends to disappear below specific sizes,[4,6] and particle morphologies.[7] It is also affected by crystallinity, defect structure, and internal strains,[8] substitution of Fe^{3+} by Al^{3+},[8] Mn^{3+},[3,9] Al^{3+}, Ga^{3+}, Cr^{3+}, and In^{3+},[10] by strains, crystal defects like low crystallinity of particles and vacancies, stoichiometric deviations and surface effects which also tend to reduce T_M,[11] doping with impurity ions,[2] radiation damages,[12] magnetic field,[3] pressure,[2,13] simultaneous action of magnetic field and pressure,[14] the presence of OH^- groups or H_2O molecules,[11] etc. The purer and better crystallized the hematite is the higher the T_M is.

T_M is usually determined from magnetization and susceptibility measurements together with other methods, like Mössbauer spectra, neutron diffraction, etc. Usually, sigmoid, *e.g.*, magnetization or susceptibility *vs.* temperature plot profiles are obtained.[15-20] They generally show a main inflection point and two tails almost parallel to the *T* axis. T_M was considered the *T* beyond which the WF phase amount becomes practically independent of *T*.[12,16,18] But since the AF and WF phases occurring in separate parts of the sample coexist[15] and participate in the equilibrium process within a *T* range,[12,14,15] T_M was also considered the *T* of the main inflection point[15,17] or that at which half of a phase is transited to the other or where half the sample is in the AF or the WF phase.[9,15]

The transition is thus characterized by a *T* region, $\Delta T = T_{M,f} - T_{M,i}$, where $T_{M,f}$ and $T_{M,i}$ are the *T*s at which the end and initiation of transition practically takes place, that may be 0.1,[3] 0.4,[6] 10 or more,[6] $\approx$13,[15] 50,[20] 70,[16,17] 100 K,[9] etc., depending on the previous nature and structure parameters and on what is specified as the initiation and end of transition. Detailed examination of results in some cases shows that ΔT can exceed 100 K.[19,20] Below and above the inflection point details may appear, not necessarily ascribed to experimental errors, while the tails, which may not be symmetrical in both directions, can show that such details and the values of parameters like magnetization, susceptibility, etc., may vary along them.[16,18,20] The equilibrium between the AF and WF phases must extend well inside the considered single AF and WF *T* regions and although an abrupt spin-flip process of all Fe^{3+} pairs was suggested by some authors,[6] ΔT is always quite large enough.

Questions for the main parameters determining the transition and its *T* region[11,21,22] are still unanswered probably because the studies concern one parameter or a limited number of them, while the transition is a thermodynamically defined process embracing many parameters. The reorientation of each pair of Fe^{3+} ions is usually considered an abrupt, instantaneous process[6] without distinct intermediate stage(s). But it is difficult to adopt that this whole complex process takes place in such a simple way and questions about the mechanism of spin reorientations *per se*[2,6,12] remain unanswered.

Electrical conductivity studies of single-crystal α-Fe_2O_3 at temperatures 100-950 K[23-26] or powder pellets[27] showed that the conductivity transition also occurs around T_M.[23-26] Much work related to the conductive behavior is focused in photoelectrochemical studies applying hematite as the photocatalyst for dissociating H_2O to convert and store solar energy,[28-35] because it has valuable properties as an oxygen photoanode.[31] Most studies examining semiconductance were made in photoelectrochemical cells[30,31,34] or in separate hematite/electrolyte systems[36] by impedance techniques. Intrinsic n-type[32] or doped n- or p-type[5,28-30,33-35] semiconductance,

[z] E-mail: gpaterma@central.ntua.gr

with a bandgap usually between 1.9 and 2.3 eV and sometimes <1.9 eV were noted. But the origin of intrinsic semiconductance and the whole conductance behavior is curiously elusive while the related derived parameters are frequently controversial. Temperatures were around the ambient one. Conductivity transition at such *T*s seems responsible for that behavior which, however, has not been discussed.

Despite the extensive work on the magnetic and electrical conductivity properties of hematite, a detailed description and explanation of conductivity transition and explanation for the co-occurrence of magnetic and conductivity transitions are absent. These may be important, besides those noted above, for other applications of hematite-like catalysis, magnetic and data media components, pigments, cooling water treatment, anticorrosive materials, etc.[17]

The scope of this study is (*i*) the detailed examination of electrical conductance transition in the spin-flip transition temperature range by impedance spectroscopy; (*ii*) the discovery of the coexistence of magnetic and electrical conductance transitions; (*iii*) the formulation of a model predicting the co-occurrence of these transitions and interpreting the conductance transition and the elusive conductive character of hematite.

Experimental

Samples of freshly prepared high purity (>99.95%) coarse grain polycrystalline α-Fe_2O_3[37,38] made of pressed powder cylindrical pellets 10 mm in diameter and a thickness of 1.6 mm by a Riken Power Press model P-1B instrument, were prepared. Two platinum foil electrodes 10 mm in diameter were adjusted on both sides of the samples and simultaneously pressed with them. Each sample was loaded into the temperature control chamber between two brass rods accompanied by a compression spring. The sample was combined in series with a resistance, $R_i = 21.5\ k\Omega$, in which the applied signal V yielded a voltage drop V_i. V_i was <0.1 V so that its effect on the phase shift was minimized.

A low-frequency dynamic signal analyzer (DSA) instrument (Hewlett-Packard model 3561A) operating in both frequency (F) and time domains ($100\ Hz \leqslant F \leqslant 100\ kHz$), applied a signal of periodic noise 72.5 mV (rms) to the system and accurately measured the amplitude and the phase (φ) relative to the trigger signal. Such data were obtained at different temperatures, *T*-190-350 K and stored for further treatment. The instrument was connected with a PC for processing the data stored in the analyzer. The detailed experimental procedure is described elsewhere.[39]

Results and Discussion

The ReZ and ImZ vs. T plots.—For the hematite sample combined with the fixed resistance R_i the equation

$$I = V(|Z| + R_i)^{-1} = V_i R_i^{-1} \text{ or}$$

$$VV_i^{-1} = (|Z| + R_i)R_i^{-1} = |Z|R_i^{-1} + 1 \text{ or } |Z| = R_i(V/V_i - 1) \quad [1]$$

is valid, where I (rms) is the current flowing through the circuit yielded by the periodic noise signal applied to the circuit having V (rms) value, Z is the impedance of sample, and V (rms) is the voltage drop in R_i. The real (ReZ) and imaginary (ImZ) parts of Z are given by the equations

$$ReZ = R_i(VV_i^{-1} - 1)\cos\varphi \quad [2]$$

$$ImZ = R_i(VV_i^{-1} - 1)\sin\varphi \quad [3]$$

while the conductivity (σ) is given from equation

$$\sigma = 4h(\pi D^2)^{-1}G = 4h(\pi D^2)^{-1}\,Re\,Z(|Z|^{-2}) \quad [4]$$

where h and D are the height and diameter of the sample and G is the conductance.

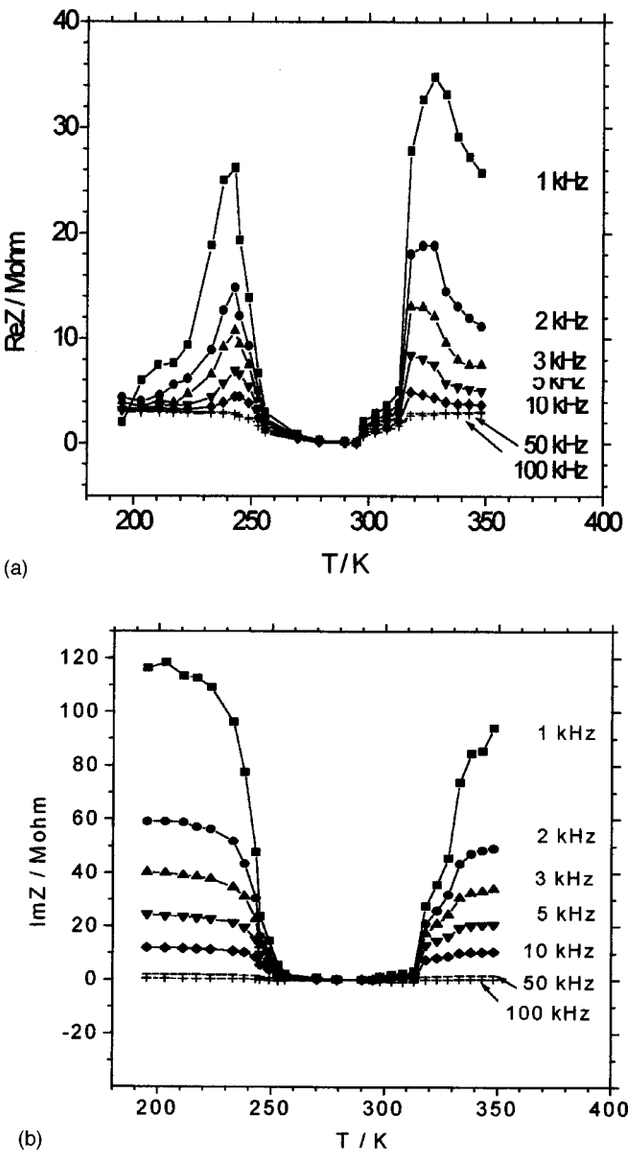

Figure 1. Plots of *ReZ* (a) and *ImZ* (b) *vs.* temperature (*T*) at different frequencies, 1, 2, 3, 5, 10, 50, and 100 kHz.

The ratio V_i (rms)/V (rms), φ and then the ReZ, ImZ, and σ were determined at different Fs and Ts. The ReZ and ImZ *vs. T* plots, Fig. 1a and b, show many details. In Fig. 1a two distinct maxima appear on either side of a well. The height of both maxima and depth of the well decrease with F. At the bottom of well the spectra converge to $1 - 5 \times 10^5\ \Omega$ values and become almost independent of F. The ImZ *vs. T* plots, Fig. 1b, show wells between the horizontal or oblique plateau, with depths decreasing with F and details qualitatively similar to those in the ReZ *vs. T* plots. At the bottom of the wells the spectra converge to an almost constant $\approx 5.4 \times 10^5\ \Omega$ value and become almost independent of F.

It is observed that the $T_M \approx 265$ K found in the literature for bulk hematite falls inside the temperature region of the deeper end of the wells of plots in Fig. 1a and b.

The complex plane plots: prediction of ion diffusion in the magnetic transition T range.—In Fig. 2a-d the ImZ *vs.* ReZ plots at $T \leqslant 249$ K (a), $256\ K \leqslant T \leqslant 290$ K (b), $T = 279$ K (c), and $T \geqslant 318$ K (d) are shown. For $T \leqslant 249$ K and $T \geqslant 318$ K on

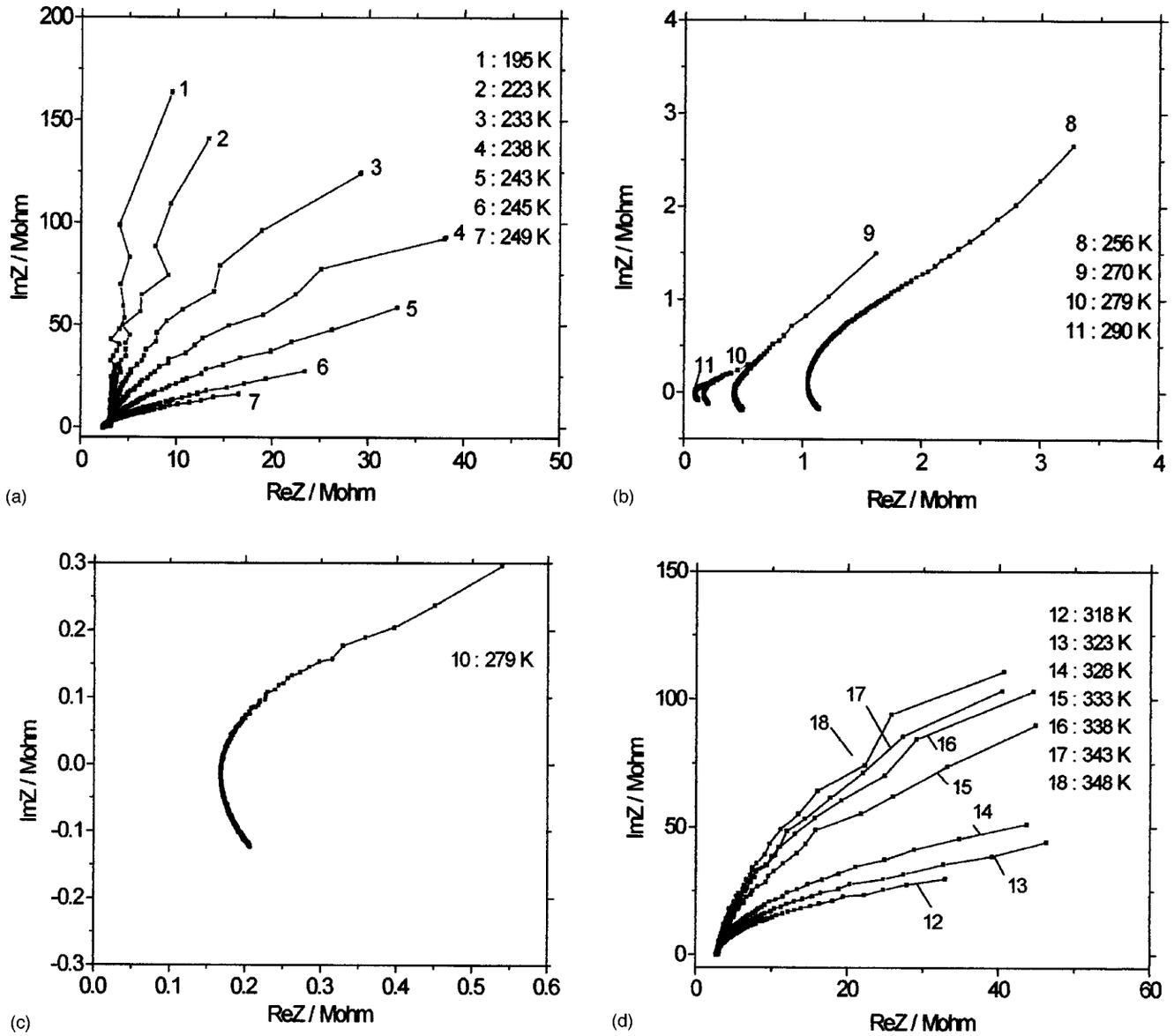

Figure 2. *ImZ vs. ReZ* plots at different temperatures (T), (a) $T \leqslant 249$ K, (b) 256 K $\leqslant T \leqslant$ 290 K, (c) $T = 279$ K, and (d) 318 K $\leqslant T \leqslant$ 348 K.

passing from low to high Fs, the plots intersect the ReZ axis at a value ≈3 MΩ almost independent of T, Fig. 2a and d. For 256 K $\leqslant T \leqslant$ 290 K, Fig. 2b, the intersection of plot with the ReZ axis decreases with T while ImZ is capacitive at low and inductive at high Fs. At low Fs the plots in Fig. 2b become linear with a 45° angle to the real axis. These become clear in the magnified plot at an intermediate $T = 279$ K, Fig. 2c. This response predicts a diffusional contribution to impedance (Warburg impedance).[36] A tendency is observed for that behavior to appear at ≈233 K, Fig. 2a and end at ≈328 K, Fig. 2d, becoming explicit around the middle of the region.

The discovery of diffusing species is important. The radii of Fe^{2+} and Fe^{3+} are 0.74 and 0.64 Å, respectively.[40] Fe^{4+} also can form relatively easily[41,42] (see also later) the radius of which must be even smaller. The radius of O^{2-} is 1.32 Å.[40] The radii of all Fe ions are much smaller than the radius of O^{2-} while their charge is equal to or higher than that of O^{2-}. Evidently coupled Fe^{3+} cannot diffuse. Only uncoupled Fe^{3+}, mainly activated as Fe^{4+} (see also below), can migrate through the available one-third vacant octahedral sites and participate in the diffusion process.

Although further research of the complex plane plots regarding the capacitive to inductive transition at high Fs, *e.g.*, by deriving an equivalent circuit, etc., may have some interest, it is outside the scope of this study in which the interest is mainly for low Fs which yielded the important information of cation diffusion involved in the following discussion.

The σ vs. T plots; comparison of Ts of conductance and magnetic transitions.—The σ *vs. T* plots, Fig. 3a and b, show almost constant σ at 190 K $< T \leqslant$ 230 K. For $T >$ 230 K an accelerated increase of σ with T is observed up to 294 K. Then, an abrupt fall of σ up to 297 K and a shoulder from 297 to ≈330 K appear. For higher Ts, σ is almost independent of T and comparable to that at $T \leqslant$ 230 K. Thus a peak arises from ≈230 to ≈330 K above a

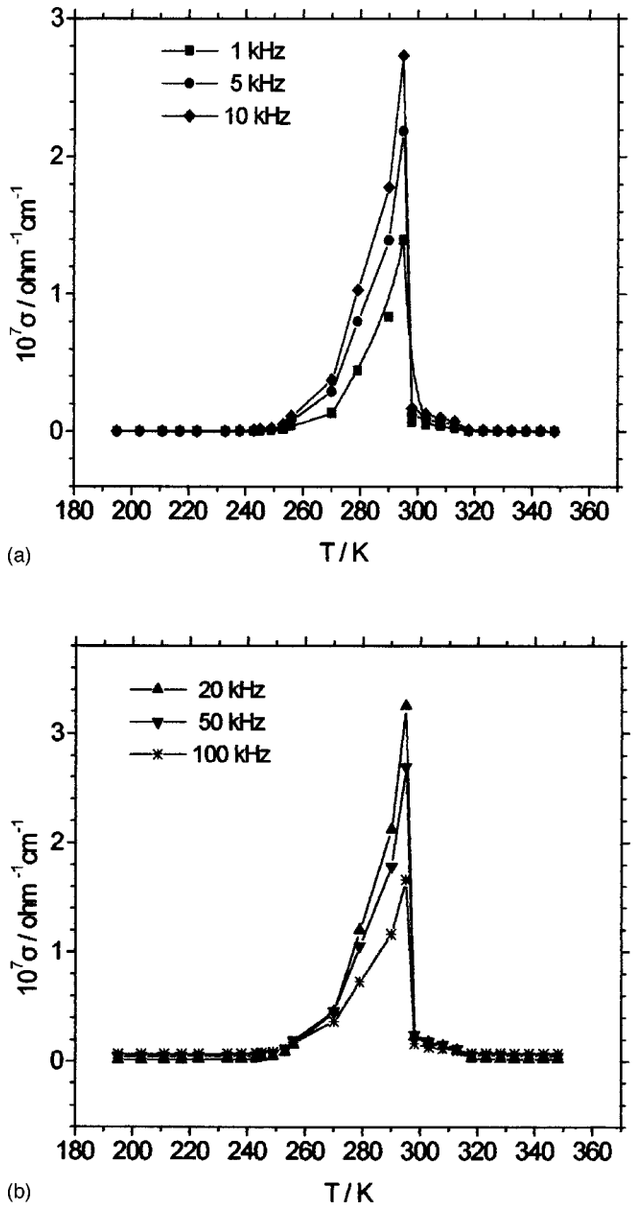

Figure 3. Plots of σ *vs.* *T* at different frequencies, (a) 1, 5, and 10 kHz and (b) 20, 50, and 100 kHz.

background of almost constant σ value at 190 K $< T \leqslant$ 230 K and 330 K $\leqslant T <$ 350 K. The T_M noted in the literature ≈265 K for bulk polycrystalline hematite falls inside the *T* region of σ rise, *i.e.*, between 230 and 294 K. Thus, it seems that the maximum σ value is met at a *T* higher than T_M while for the hematite sample used $T_{M,i} \approx 230$ K, $T_{M,f} \approx 330$ K, and $\Delta T = T_{M,f} - T_{M,i} \approx 100$ K in agreement to earlier results.[9,19,20]

At $T \leqslant T_{M,i}$ and $T \geqslant T_{M,f}$ the plots are slightly shifted upwards with *F*. At $T_{M,i} < T < T_{M,f}$ the peak seems to pass through a maximum at about $F = 20$ kHz. Besides the above, other complementary details and information are derived below from the $\ln\sigma$ *vs.* $10^3\ T^{-1}$ plots.

The $\ln\sigma$ *vs.* $10^3\ T^{-1}$ *plots; characterization of conductance at* $T < T_{M,i}$ *and* $T > T_{M,f}$.—The $\ln\sigma$ *vs.* $10^3\ T^{-1}$ plots at different *F*s are shown in Fig. 4. A background is observed for $T \leqslant T_{M,i}$ and $T \geqslant T_{M,f}$ above which a peak appears between $T_{M,i}$ and $T_{M,f}$. The plot points on the left and right of the peak seem to belong to the same straight line, except for the last right point in Fig. 4a which deviates, apparently due to experimental errors because such a behavior is not observed at other *F*s. The increase of $\ln\sigma$ of background with *T* implies the occurrence of a semiconductance. For a single semiconduction mechanism of any type at *T*s below the saturation one, the equation

$$\sigma = \sigma_0 \exp(-E_a/2kT) \quad \text{or} \quad \ln\sigma = \ln\sigma_0 - E_a/2kT \qquad [5]$$

must apply where σ_0 is a constant, almost independent of *T*, proportional to the number (or concentration) of species implicitly activated, E_a is the energy barrier, and *k* is the Boltzmann constant. For intrinsic semiconductance $E_a = E_g/2$, where E_g is the bandgap. E_a was found to vary from 0.12 eV at $F = 1$ kHz to almost 0 at $F = 100$ kHz. This small E_a predicts a doping donor or acceptor activation and that semiconductance is due to traces of impurities. The increase of σ with *F* may be due to an increase of carrier mobilities with *F* which is also reflected as a decrease of E_a. This conductivity cannot be ascribed to ionic conduction as a main component since E_a should be comparable to 0.5 eV.[43]

The peak shows many details and like breaking or inflection points denoting a complex variation of $\ln\sigma$ with $10^3\ T^{-1}$. On its right side two such characteristic points appear, A and B at ≈230 K ($10^3\ T^{-1} = 4.35\ \text{K}^{-1}$) and ≈260 K ($10^3\ T^{-1} = 3.85\ \text{K}^{-1}$) for $F = 1$ kHz. On its left side three inflection points appear. In both regions σ cannot be described by simple formulas. Figure 4 confirms that the Morin transition *T* region practically extends from ≈230 to ≈330 K.

A simple model, thermodynamically sustained, describing the magnetic transition.—As shown in the Morin transition *T* region the AF and WF phases coexist in an equilibrium AF ⇄ WF.[12,14,15] The results presented here are consistent with that the transition AF ⇄ WF does not take place directly through a single specific activated complex state, which probably requires a prohibitively high activation energy, but, instead, it takes place through another phase, that of uncoupled ions, UIP, in which the separate spins are oriented to different directions, other than parallel to the [111] axis or the (111) plane characteristic for AF and WF coupling. It thus follows the scheme AF ⇄ UIP ⇄ WF. Hence, two separate partial equilibrium processes coexist

$$\text{AF} \rightleftarrows \text{UIP} \quad \text{or} \quad [\text{Fe}^{3+}{}_{\text{SL1}}\downarrow\uparrow\text{Fe}^{3+}{}_{\text{SL2}}]_0{}^{\text{o}} \rightleftarrows \text{Fe}^{3+}{}_{\text{SL1}} + \text{FE}^{3+}{}_{\text{SL2}} \qquad [6]$$

$$\text{UIP} \rightleftarrows \text{WF} \quad \text{or} \quad \text{Fe}^{3+}{}_{\text{SL1}} + \text{Fe}^{3+}{}_{\text{SL2}} \rightleftarrows [\text{Fe}^{3+}{}_{\text{SL1}}\downarrow\uparrow\text{Fe}^{3+}{}_{\text{SL2}}]_{90}{}^{\text{o}} \qquad [7]$$

where SL1 and SL2 are the alternative sublattices and indexes 0° and 90° are the angles of magnetic moments of coupled ions with the [111] axis. It is considered that the bulk concentration of uncoupled Fe^{3+} pairs is C_{UIP} while that of AF and WF coupled Fe^{3+} pairs is C_{AF} and C_{WF}, respectively. Then $C_{AF} + C_{WF} + C_{UIP} = C_0$ (constant concentration of Fe atom pairs). Apparently the parts of sample in the AF and WF phases are proportional to C_{AF} and C_{WF}, respectively.

Processes 6 and 7 are thermally activated. The equilibrium state is characterized by certain concentrations of involved species depending on *T*. The C_{AF} and C_{WF} must decrease and increase, respectively, with *T* until the AF and UIP phases are almost completely depleted at $T > T_{M,f}$.

Because the lattice positions of O^{2-} and the middle of the distances between Fe^{3+} in each pair remain almost unchanged during magnetic transition, the change of lattice energy can be almost exclusively attributed to the change of the state of Fe^{3+} pairs. Then, the magnetic transition process can be schematically depicted regarding the energy of each phase (*E*) as in Fig. 5. On passing from AF through UIP to the WF phase the energy increases while the

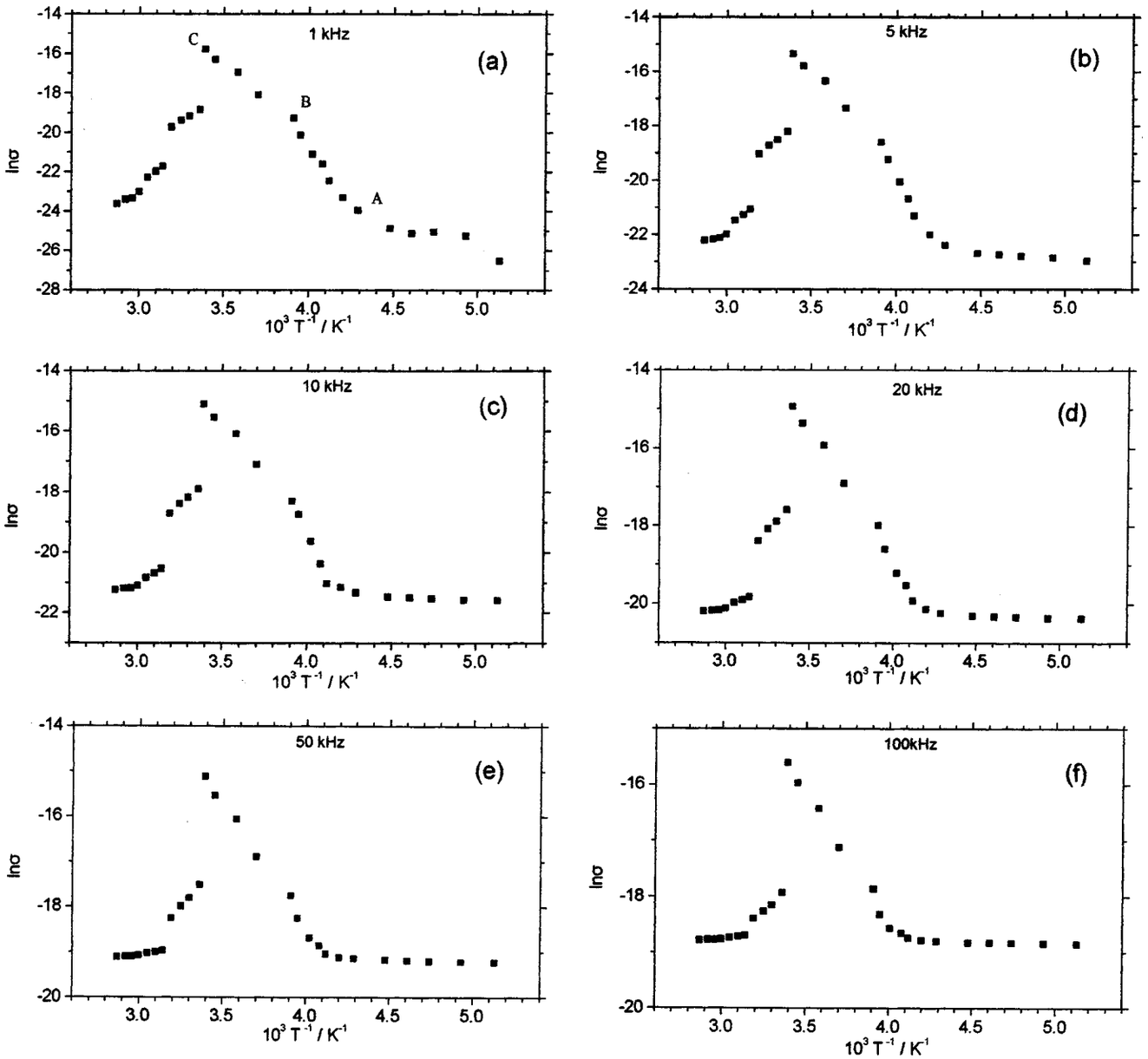

Figure 4. Plots of $\ln \sigma$ *vs.* $10^3\ T^{-1}$ at different frequencies, (a) 1, (b) 5, (c) 10, (d) 20, (e) 50 and (f) 100 kHz.

energy hills between successive phases represent the phase transitions through suitable activated complexes the energy of which corresponds to hilltops. That diagram is consistent with earlier results[44] for the AF and WF phases supporting that AF is more stable. The uncoupling process and UIP phase are also somehow predicted[44] because a large charge transfer from O^{2-} to $3d^5$ Fe^{3+}, leading to a smaller magnetic moment, occurs, thus assisting uncoupling. From the activated complex theory,[45] the activation energies of the right and left directed processes in Eq. 6 and 7 are $E_{1,r} > E_{1,l}$ and $E_{2,r} > E_{2,l}$, *i.e.*, they are endothermic with standard enthalpies $\Delta H^0{}_{T,1} = E_{1,r} - E_{1,l} > 0$ and $\Delta H^0{}_{T,2} = E_{2,r} - E_{2,l} > 0$. The equilibrium constants are

$$k_1 = C_{UIP}/C_{AF} = \exp(\Delta S^0{}_{T,1}/R)\exp(-\Delta H^0{}_{T,1}/RT) \quad [8]$$

$$k_2 = C_{WF}/C_{UIP} = \exp(\Delta S^0{}_{T,2}/R)\exp(-\Delta H^0{}_{T,2}/RT) \quad [9]$$

where $\Delta S^0{}_{T,1}$ and $\Delta S^0{}_{T,2}$ are the changes of standard entropies.

For convenience it was adopted that in the not excessively large range of Ts employed, $\Delta H^0{}_{T,1}$, $\Delta S^0{}_{T,1}$, $\Delta H^0{}_{T,2}$, and $\Delta S^0{}_{T,2}$ are independent of T and equal to the standard values at $T = 298$ K, $\Delta H^0{}_1$, $\Delta S^0{}_1$, $\Delta H^0{}_2$, and $\Delta S^0{}_2$. Since the AF and WF states are more ordered than UIP, then $\Delta S^0{}_{T,1} > 0$ and $\Delta S^0{}_{T,2} < 0$. Because $\Delta H^0{}_{T,1} > 0$ and $\Delta H^0{}_{T,2} > 0$, k_1 and k_2 must be negligible at low Ts and quickly increase with T.

From equation $C_0 = C_{AF} + C_{WF} + C_{UIP}$ and Eq. 8 and 9

$$C_{AF} = C_0/(1 + k_1 + k_1k_2),$$

$$C_{WF} = C_0/[1 + (k_1{}^{-1} + 1)/k_2],$$

$$\text{and } C_{UIP} = C_0/(1 + k_1{}^{-1} + k_2) \quad [10]$$

An analytical research of these last equations for the variation of C_{AF}, C_{WF}, and C_{UIP} with T is difficult or even impossible. But their variations are easily derived as follows.

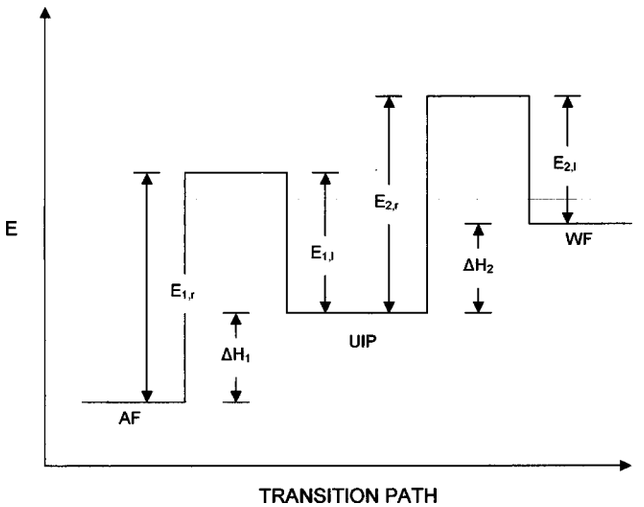

Figure 5. Schematic energy diagram during transition from AF to WF phase through the UIP in which the activation energies of the forward and reverse processes and the enthalpies are distinguished.

The exponential T dependence of k_1 and k_2 and Eq. 10 predict that C_{AF} and C_{WF} decreases and increases, respectively, with T. At low and high enough Ts $C_{WF} \rightarrow 0$ and C_0, respectively. As T becomes low and high enough C_{WF} tends to be asymptotic parallel to the T axis cutting the C_{WF} axis at 0 and C_0, respectively. Hence the C_{WF} *vs.* T plot has a sigmoid profile with two tails and an inflection point, as indeed is observed in the magnetization and susceptibility *vs.* T plots.[15,17,17-20] The inflection point cannot be found analytically except for the case where C_{UIP} is negligible compared to $C_{AF} + C_{WF}$. From Eq. 8 and 9 $k_1k_2 = C_{WF}/C_{AF} \approx C_{WF}/(C_0 - C_{WF})$ and $C_{WF} \approx C_0/[1 + 1/(k_1k_2)]$. The condition for the appearance of the inflection point, $d^2C_{WF}/dT^2 = 0$, is satisfied when

$$-(\Delta S^0{}_1 + \Delta S^0{}_2) + (\Delta H^0{}_2 + \Delta H^0{}_1)/T = 0 \qquad [11]$$

Since $(\Delta H^0{}_2 + \Delta H^0{}_1) > 0$, then $-(\Delta S^0{}_1 + \Delta S^0{}_2) < 0$ which denotes that the AF state is more ordered than the WF, as expected, verifying the above analysis. Probably C_{UIP} is indeed small enough (which occurs when $k_1{}^{-1} + k_2 \gg 1$) justifying the fact that the UIP state, as an intermediate one between AW and WF, was not detected by other methods and therefore is not noted in the literature.

Similarly, it is found that the C_{AF} *vs.* T plot has an inverse sigmoid profile with two tails tending at low and high Ts to asymptotes parallel to the T axis and cutting the C_{AF} axis at C_0 and 0, respectively.

When T decreases, k_1 and k_2 quickly decrease, due to their exponential T dependences, so that k_1 becomes $\ll 1$, and therefore $k_1{}^{-1} \gg 1$, and $C_{UIP} \rightarrow 0$, Eq. 10. As T increases k_1 and k_2 quickly increase so that k_2 becomes $\gg 1$ and $C_{UIP} \rightarrow 0$. Hence, at low and high enough Ts $C_{UIP} \rightarrow 0$. It is noted that these limiting inequalities are consistent with the previous one, $k_1{}^{-1} + k_2 \gg 1$ for each T. Thus, C_{UIP} passes through a maximum at a T for which $dC_{UIP}/dT = 0$ or when

$$-k_1{}^{-1}\Delta H^0{}_1 + k_2\Delta H^0{}_2 = 0 \qquad [12]$$

which is plausible, since $\Delta H^0{}_1$ and $\Delta H^0{}_2 > 0$, also verifying the above analysis. Thus, the C_{UIP} *vs.* T plot has a bell-like profile. Apparently, when $\Delta H^0{}_{T,1}$, $\Delta S^0{}_{T,1}$, $\Delta H^0{}_{T,2}$, and $\Delta S^0{}_{T,2}$, which actually depend slightly on T, are taken into consideration, additional details in the above, *e.g.*, C_{WF} and C_{UIP} *vs.* T, plots can appear. Those of the first plot case can explain details in magnetization or susceptibility *vs.* T plots.[5,6,10] As observed the model is strictly thermodynamically sustained and consistent.

Characterization of conductance at $T_{M,i} < T < T_{M,f}$ and interpretation of σ peak and co-occurrence of conductive and magnetic transitions by the previous model. Uncertainty for determining activation energy and bandgap values from the $\ln\sigma$ *vs.* $10^{-3}\ T^{-1}$ *plots.*—There is strong evidence that the peak conductivity at $T_{M,i} < T < T_{M,f}$ is predominantly due to intrinsic semiconductance. Although electronic and band structure studies showed that the valence band is formed from occupied e_g Fe 3d orbitals with a strong antibonding admixture of O 2p and the conduction band-edge forms from the t_{2g} levels of Fe 3d and O 2p, a simple model explaining the conductance data is absent.[34] Optical studies supported the process $2Fe^{3+} + 2.1\ eV \rightarrow Fe^{4+} + Fe^{2+}$ and a two-carrier semiconductance for undoped hematite.[41,42] Fe^{4+} and Fe^{2+} concern valence band holes and species enriched with electrons of conduction band. The results agree with this process which justifies both the intrinsic semiconductance and formation of the aforementioned diffusing ions.

The intrinsic activation concerns a fraction of UIP Fe^{3+} and therefore σ is given by equation

$$\sigma = \sigma_0{}'C_{UIP}\exp(-E_a/2kT) \qquad [13]$$

where $\sigma_0{}'$ is a constant, almost independent of T. It is evident that σ is defined by C_{UIP} which varies with T, according to a bell-like profile and by the factor $\exp(-E_a/2kT)$ for which the rise of T causes an accelerated increase. Thus, σ must show a peak with a maximum value at a T higher than that of the maximum C_{UIP} value, while the peak must be not symmetrical, as indeed is observed in Fig. 3 and 4.

Since C_{UIP} varies with T, treatment of σ values by Eq. 5 cannot yield the true E_a and E_g values. An elucidative example is given. From the approximately linear part of plots between 230 K ($10^3\ T^{-1} = 4.35\ K^{-1}$) and 260 K ($10^3\ T^{-1} = 3.85\ K^{-1}$), region AB in Fig. 4, the E_a, calculated by Eq. 5, is 1.1505 eV at $F = 1$ kHz and therefore, supposing that this corresponds to the intrinsic activation energy, $E_g = 2E_a = 2.31$ eV. It decreases with F due, apparently, to its effect on carrier mobilities which are reflected as a variation of E_a. Between 260 K ($10^3\ T^{-1} = 3.85\ K^{-1}$) and 294 K ($10^3\ T^{-1} = 3.40\ K^{-1}$), region BC in Fig. 4, Eq. 5 gives E_a varying from 0.58 to 0.38 eV and E_g from 1.16 to 0.76 eV for $F = 1$-100 kHZ. Calculation of E_a in the range AC, 230-294 K, considering a rough linearity gives, at, *e.g.*, $F = 1$ kHz, $E_a = 0.78$, and $E_g = 1.56$ eV. Similar treatment of results in a T region extending, *e.g.*, from a T, 294 K $\geqslant T \geqslant$ 260 K, to a $T > 294$ K yields totally misleading and unrealistic conclusions.

Recent results for a pellet hematite sample in the T region from ≈285 to ≈305 K[27] gave an $\ln\sigma$ *vs.* $10^3\ T^{-1}$ plot curving upwards, as observed on average in plots of Fig. 4 in the right side of the peak, and σ of the same order as here in this T region. This denotes that the σ peak in that sample must appear at a T higher than here, apparently due to its different composition, *e.g.*, less purity, 99.124%, etc. The estimated E_a, 0.735 eV, is close to the previous average one found in the right side of the peak in the $\ln\sigma$ *vs.* $10^3\ T^{-1}$ plot for $F = 1$ kHz, 0.78 eV, also validating the present analysis.

Hence, the real constant E_a and E_g values cannot be found by Eq. 5 since they depend strongly on the T range examined. Considering that the AB region, Fig. 4, corresponds to the left tail of the bell-like C_{UIP} *vs.* T plot, where C_{UIP} does not largely vary, then 1.1505 and 2.31 eV can be considered only rough estimates of E_a and E_g. E_gs found in earlier studies, varying from 2.3 to below 1.9 eV as previously noted, lie between the values 2.31 and 1.56 eV, given previously, which as shown above are inaccurate. The strong differences met in the literature for E_a, *e.g.*, 2.1 eV[41,42] or 0.735 eV[27] and for E_g varying as above or 3.36 eV[46] are thus justified by Eq. 13, the

variation of C_{UIP} (or of the implicitly activated species) with T and the different T ranges examined.

The C_{UIP} must become maximum at a T, which can be considered $\approx T_M$, between 260 and 294 K, *i.e.*, around 278 K, which is close to the 265 K in the literature for bulk hematite. Details of σ (or $\ln \sigma$) *vs.* T plots are explained by the aforementioned details of the C_{UIP} *vs.* T plot. Occurrence of an appreciable contribution of ionic conduction is not excluded. As shown, ionic transport occurs at Ts from $T_{M,i}$ to $T_{M,f}$. Ionic diffusion is favored by high C_{UIP}s, or in the T range of magnetic transition. The ionic contribution must also obey a relationship similar to Eq. 13. Although the results cannot prohibit a significant ionic contribution to conductance, because the real E_a, comparable to 1.1505 eV, is much higher than $\approx$0.5 eV[43] characterizing diffusional processes in solid state, intrinsic semiconductance is the main contribution. The maximum in σ peak around $F = 20$ kHz, Fig. 3, can be attributed to different effects of F on carriers mobilities in intrinsic and ionic contribution to conductance.

The significance and further consequences of the derived results.—The real $T_{M,f} - T_{M,i}$ range is accurately defined by this method, without measuring magnetization and its variation with T. The results showed that IS can be applied to study the magnetic properties of some materials as well as the electrical properties. An effective method for such studies is thus introduced.

As shown, the conductance behavior is complex enough at $T_{M,i} < T < T_{M,f}$. If details on the kind of conductance and effects of parameters like T and F on σ cannot be suitably distinguished by the method employed, conclusions derived in investigations in which conductance is involved will be misleading. Treatment of results at Ts in the range from $T_{M,i}$ to $T_{M,f}$ considering simple semiconductive character, following, *e.g.*, Eq. 5, cannot precisely determine the conduction character, bandgap, and other related parameters and therefore the total photocatalytic behavior[28-35] for which the ion diffusion processes may also affect carrier recombinations yielding low efficiency. That Ts and the complex conductance character of hematite are important for such studies. To optimize efficiency, conductance, and magnetic transitions, ion diffusion and related Ts must be taken into consideration. Similar observations can be made for other applications of hematite as well.

Conclusions

From the results of this study the following concluding remarks can be drawn:

The application of IS to hematite at 190-350 K revealed a complex behavior. A background of σ out of the magnetic transition T range appears and a peak of σ appears within this T range. The spin-flip transition and its T range, $\approx$230 $-$ $\approx$330 K, corresponding to the region of appearance of conductivity peak, were precisely predicted.

A model, thermodynamically sustained and therefore strict with an uncontested validity, was formulated interpreting, for first time, the coexistence and interaction of magnetic and conductance transitions. It predicts that the peak of conductivity is due to the appearance of a peak of bulk concentration of uncoupled Fe^{3+} and the exponentially T-dependent fraction of activated Fe^{3+} yielding primarily intrinsic conduction. Magnetic and conductance transitions occur over a relatively large T range as a result of equilibrium processes 6 and 7.

The formulated model for co-occurring complex conductance and magnetic transitions can explain the, so far, elusive semiconductance and controversial behavior of hematite in some applications.

Although the formulated model is consistent with the results in each case and no contradiction was observed or can be conceived, verifying its validity, further investigation along the lines of this study on the intermediate phase of uncoupled Fe^{3+} ions between the AF and WF phases is necessary to fully elucidate the concurrency of the electric and magnetic transitions.

Acknowledgments

The authors thank Dr. Anthoula Dimirkou, member of the Soil Science Institute of Athens, for the gift of the hematite samples.

The authors assisted in meeting the publication costs of this article.

References

1. J. O. Artman, J. C. Murphy, and S. Foner, *Phys. Rev.* **138**, A912 (1965).
2. K. M. Creer, I. G. Hedley, and W. O'Reilly, in *Magnetic Oxides*, Part 2, D. J. Craik, Editor, p. 664, John Wiley & Sons, London (1975).
3. C. Leycuras, H. Le Gall, D. Minella, E. G. Rudashewsky, and V. S. Merkoulov, *Physica B & C*, **89**, 43 (1977).
4. W. Kündig, H. Bömmel, G. Constabaris, and R. H. Lindquist, *Phys. Rev.*, **142**, 327 (1966).
5. N. Amin and S. Arajs, *Phys. Rev. B*, **35**, 4810 (1987).
6. R. C. Nininger, Jr., and D. Schroeer, *J. Phys. Chem. Solids*, **39**, 137 (1978).
7. M. Sorescu, R. A. Brand, D. Mihaila-Tarabasanu, and L. Diamandescu, *J. Appl. Phys.*, **85**, 5546 (1999).
8. E. De Grave, L. H. Bowen, R. Vochten, and R. E. Vandenberghe, *J. Magn. Magn. Mater.*, **72**, 141 (1988).
9. R. E. Vandenberghe, A. E. Verbeeck, and E. De Grave, *J. Magn. Magn. Mater.*, **54-57**, 898 (1986).
10. E. Sváb and E. Krén, *J. Magn. Magn. Mater.*, **14**, 184 (1979).
11. M. Z. Dang, D. G. Rancourt, J. E. Dutrizac, G. Lamarche, and R. Provencher, *Hyperfine Interact.*, **117**, 271 (1998).
12. Ö. F. Bakkaloglu and M. F. Thomas, *J. Magn. Magn. Mater.*, **104**, 1921 (1992).
13. C. L. Bruzzone and R. Ingalls, *Phys. Rev. B*, **28**, 2430 (1983).
14. V. V. Nitts, *Solid State Commun.*, **30**, 71 (1979).
15. V. V. Kvardakov, J. Sandonis, K. M. Podurets, S. S. Shilstein, and J. Baruchel, *Physica B*, **168**, 242 (1991).
16. K. K. Sahu, C. Rath, N. C. Mishra, S. Anand, and R. P. Das, *J. Colloid Interface Sci.*, **185**, 402 (1997).
17. M. Vasquez-Mansilla, R. D. Zysler, C. Arciprete, M. Dimitrijewits, D. Rodriguez-Sierra, and C. Saragovi, *J. Magn. Magn. Mater.*, **226**, 1907 (2001).
18. R. C. Plaza, S. A. Gómez-Lopera, and A. V. Delgado, *J. Colloid Interface Sci.*, **240**, 48 (2001).
19. M. Vasquez-Mansilla, R. Zysler, D. Fiorani, and L. Suber, *Physics B*, **320**, 206 (2002).
20. S. J. Stewart, R. A. Borzi, E. D. Cabanillas, G. Punte, and R. C. Mercader, *J. Magn. Magn. Mater.*, **260**, 447 (2003).
21. R. E. Vandenberghe, E. De Grave, C. Landuytdt, and L. H. Bowen, *Hyperfine Interact.*, **53**, 175 (1990).
22. T. Fujii, M. Takano, R. Kakano, Y. Isozumi, and Y. Bando, *J. Magn. Magn. Mater.*, **135**, 231 (1994).
23. J. Morin, *Phys. Rev.*, **83**, 1005 (1951).
24. J. Martinet, *Compt. Rend.*, **234**, 2167 (1952).
25. A. K. Mukerjee, *Indian J. Phys.*, **42**, 673 (1968).
26. A. K. Mukerjee, *Indian J. Phys.*, **43**, 230 (1969).
27. N. Guskos, G. J. Papadopoulos, V. Likodimos, S. Patapis, D. Yarmis, A. Przepiera, K. Przepiera, J. Majszczyk, J. Typek, M. Wabia, K. Aidinis, and Z. Drazek, *Mater. Res. Bull.*, **37**, 1051 (2002).
28. J. H. Kennedy, R. Shinar, and J. P. Ziegler, *J. Electrochem. Soc.*, **127**, 2307 (1980).
29. R. Shinar and J. H. Kennedy, *J. Electrochem. Soc.*, **130**, 860 (1983).
30. J. E. Turner, M. Hendewerk, J. Parmeter, D. Neiman, and G. A. Somorjai, *J. Electrochem. Soc.*, **131**, 1777 (1984).
31. L. C. Schumacher, S. Mamiche-Afara, M. F. Weber, and M. J. Dignam, *J. Electrochem. Soc.*, **132**, 2945 (1985).
32. J. K. Leland and A. J. Bard, *J. Phys. Chem.*, **91**, 5076 (1987).
33. J. Leduc and S. M. Ahmed, *J. Phys. Chem.*, **92**, 6661 (1988).
34. S. M. Ahmed, J. Leduc, and S. F. Haller, *J. Phys. Chem.*, **92**, 6655 (1988).
35. N. J. Cherepy, D. B. Liston, J. A. Lovejoy, H. Deng, and J. Z. Zhang, *J. Phys. Chem. B*, **102**, 770 (1998).
36. B. D. Cahan and C. T. Chen, *J. Electrochem. Soc.*, **129**, 474 (1982).
37. W. R. Fisher and U. Schwertmann, *Clays Clay Miner.*, **23**, 33 (1975).
38. A. Dimirkou, A. Ioannou, and Ch. Kallianou, *Commun. Soil Sci. Plant Anal.*, **27**, 1091 (1996).
39. J. Papaioannou, N. Papadimitropoulos, and I. Mavridis, *Mol. Phys.*, **97**, 611 (1999).
40. *Handbook of Chemistry and Physics*, R. C. Weast, Editor, 60th ed., p. F-214, CRC Press, Boca Raton, FL (1979).
41. D. Benjelloun, J. P. Bonnet, and M. Onillon, in *Transport in Non-Stoichiometric Compounds*, V. S. Stubican and G. Simkovich, Editors, p. 198, Plenum Press, New York (1983).
42. C. V. Santilli, J. P. Bonnet, P. Dordor, and M. Onillon, *J. Mater. Sci.*, **28**, 6029 (1993).
43. Ch. Kittel, *Introduction to Solid State Physics*, 3rd ed., p. 570, John Wiley & Sons, New York (1968).
44. M. Catti, G. Valerio, and R. Dovesi, *Phys. Rev. B*, **51**, 7441 (1995).
45. P. W. Atkins, *Physical Chemistry*, 3rd ed., p. 745, Oxford University Press, New York (1986).
46. G. V. Samsonov, *The Oxide Handbook*, p. 309, IFI/Plenum, New York (1973).